2. Experimental

Introduction

The purpose of this chapter is to present the experimental details of this study. This chapter is divided into three main parts, which discuss the preparation of WO_3 nanocrystalline powder, the experimental techniques used to analyse the structural properties of the WO_3 powders and the implementation and test of gas sensor devices. For the sake of brevity, this chapter just gives the main information needed to understand the research carried out in this study. It is not the scope to give complete and detailed information about sample preparation or characterisation techniques. Excellent books and reviews have been written, and are here cited, if the reader is interested in obtaining a deeper view of a particular field. That is why most of the references found in this chapter are not inserted in the text, as usual, but they are gathered at the end of the corresponding subsection.

The first section reports on the chemical route followed to obtain pure and catalysed WO_3 nanocrystalline powders.

The second part deals with the description of the characterisation techniques used in this work. Some of these techniques, such as X-ray diffraction, X-ray photoelectron spectroscopy, Transmission electron microscopy or Raman spectroscopy, have been used rather as routinely characterisation techniques and, in fact, they have been widely described in previous works concerning the characterisation of nanocrystalline powders for gas sensors in our research group. Therefore, more emphasis is placed on the rest of techniques (Temperature programmed desorption, Electron paramagnetic resonance and Diffuse reflectance spectroscopy). These are not new techniques at all, of course, but they are not so common in the field nanocrystalline metal oxides applied to gas sensors, so more details are provided.

Finally, the third part describes the fabrication of gas sensors from nanocrystalline WO_3-based powder and their test. As in the previous section, the preparation and test of similar sensors has been also very well reported in previous works, so only a short description is provided.

2.1 Sample preparation

Nanocrystalline tungsten trioxide was prepared following a soft chemistry route, classified as a sol-gel route by some authors, from tungstic acid (H_2WO_4). This route has been applied in catalysis [1,2] and, to the best of our knowledge, it had never been used before for gas sensing applications, where the pyrolisis of ammonium paratungstate is much more common [3,4].

Typically, tungstic acid (10.0 g) was dissolved in 31.0 ml of methanol (Fig. 1). After stirring at room temperature for 15 minutes, 18.0 ml of water (1:25 tungstic acid:water molar ratio) were slowly dropped into the tungstic acid-methanol solution, which was refluxed at 80°C for 20 hours under stirring in air. Afterwards, it was dried in vacuum and the obtained powder was further treated for 5 hours at 110 °C in air. Nanocrystalline WO_3 was obtained by annealing the dried powder between 400°C or 700°C for 5 hours, under a flow of synthetic air (50-ml min^{-1}).

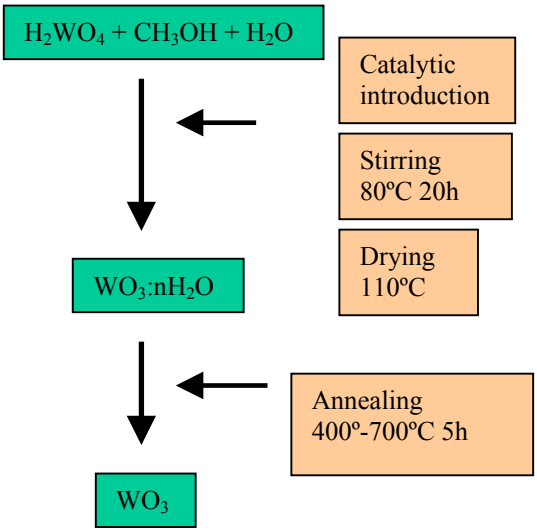

Fig. 1: *Chemical route followed in this work to obtain nanocrystalline WO_3-based powder*

Copper, chromium and vanadium catalysed WO_3 (metal:W atomic ratios 0.2, 1, 2 and 5%) were prepared by adding the stoichiometric amount of monohydrate copper acetate, chromium nitrate nonahydrate (both dissolved in methanol) and ammonium metavanadate (dissolved in aqueous oxalic acid, 10^{-4}M, solution) to the tungstic acid-methanol solution before heating at 80 °C. The remaining steps were followed as previously explained (Fig. 1). Hereafter, copper catalysed WO_3 with a Cu/W ratio of 0.2% will be labelled as WO_3:Cu(0.2%) and so on for the rest of materials.

2.2 Characterisation techniques

2.2.1 X-ray diffraction

This technique allows identifying and studying crystalline materials by using the phenomenon of diffraction. Briefly, diffraction occurs when penetrating radiation, such as X-rays, enters a crystalline substance and is scattered. The direction and intensity of the scattered (diffracted) beams depends on the orientation of the crystal lattice with respect to the incident beam. Any face of a crystal lattice consists of parallel rows of atoms separated by a unique distance (d-spacing), which are capable of diffracting X-rays. In order for a beam to be 100% diffracted, the distance it travels between rows of atoms at the angle of incidence must be equal to an integral multiple of the wavelength of the incident beam. D-spacings that are greater or lesser than the wavelength of the directed X-ray beam at the angle of incidence will produce a diffracted beam of less than 100% intensity. The resulting analysis is described graphically as a set of peaks with intensity on the Y-axis and goniometer angle on the X-axis

If the sample is powdered, it provides, theoretically, all possible orientations of the crystal lattice, the goniometer provides a variety of angles of incidence, and the detector measures the intensity of the diffracted beam. The exact angle and intensity of a set of peaks is unique to the crystal structure being examined. A comparison with patron tables, such as JCPDS spectra published by the American Society for Testing and Materials, provides valuable information about the composition of the powder.

Besides, XRD can be used to determine the crystallite size of the sample, which is a key point in the field of gas sensors based on metal oxides. Nano-sized crystals are generally too fine to be measured by light microscopy. Laser scattering methods give only average particle sizes; therefore particle size can not be measured in a particular crystallographic direction. Moreover, the particles measured by laser techniques may be composed of several different minerals, and may be agglomerations of individual crystals. Measurement by electron and atomic force microscopy is tedious, expensive and time consuming. It is difficult to measure more than a few hundred particles per sample by these methods. This many measurements, often taking several days of intensive effort, may yield an accurate mean size for a sample, but may be too few to determine an accurate distribution of sizes.

Measurement of size distributions by X-ray diffraction (XRD) solves these shortcomings. An X-ray scan of a sample occurs automatically, taking a few minutes to a few hours and the resulting XRD peaks average diffraction effects from billions of individual nano-sized crystals. The simplest approach is to use the peak breadth at half maximum (FWHM) and the Scherrer equation. However, the size that is measured by XRD may be related to the size of the individual crystals of the mineral in the sample, rather than to the size of particles formed from the agglomeration of these crystals. Moreover, crystalline defects can mislead the measurement of the crystallite size based on the Scherrer equation. These shortcomings make necessary to use other techniques to check XRD results.

In this investigation, information about the crystalline structure of the powders and their crystallite size has been obtained from XRD data. The patterns of the nanopowders were obtained with a Siemens D-500 X-ray diffractometer using Cu-Kα radiation, with operating voltage of 40 kV and current of 30 mA Further information about this technique and its application to nanocrystalline powder can be found elsewhere [5-7].

2.2.2 Transmission electron microscopy

In Transmission electron microscopy (TEM), electrons focused by condenser lenses collide with the sample and are dispersed. An image is obtained from those less dispersed and it is successively magnified by electromagnetic lenses. Finally, it is projected onto an electron sensitive film or a screen. In this work, three main features have been investigated by this technique: size and shape of the WO_3 nanoparticles, crystalline structure and defects and, finally, distribution of the catalytic additive over the tungsten oxide particle.

Conventional TEM under bright field conditions is used for determining the size and shape of nanoparticles. The direct electron beam, not scattered, is selected from the diffraction pattern with the objective aperture. Aspects of this technique [8], as well as a complete description of its application to nanopowders for gas sensing applications [9], can be found elsewhere.

High resolution TEM (HRTEM) is a powerful technique for the structural study of the nanocrystalline samples. Images can be digitally processed and compared with computer simulations. More information about its application to the field of catalysis and gas sensors is available in [10,11].

The measurement of the electron energy loss gives information about the chemical nature of the sample. One of the possible forms to analyse this is studying the distribution of electrons that have interacted inelastically with the specimen and passed through it, which is known as Electron energy-loss spectrometry (EELS). It is possible to detect light elements and their electronic structure, bonding and nearest-neighbour distribution.

For this study, aspect and grain size of the powders, crystalline structure and defects have been investigated by HRTEM, whereas EELS has provided information about the distribution of the additives on WO_3 when possible. More information about these techniques can be found in [8].

2.2.3 X-ray Photoelectron Spectroscopy

X-ray Photoelectron Spectroscopy known as XPS or ESCA (Electron Spectroscopy for Chemical Analysis) has the ability to measure binding energy variations resulting from their chemical environment. Photoelectron spectroscopy utilises photo-ionisation and energy-dispersive analysis of the emitted photoelectrons to study the composition and electronic state of the surface region of a sample.

Photoelectron spectroscopy is based upon a single photon in/electron out process. In XPS the photon is absorbed by an atom in a molecule or solid, leading to ionisation and the emission of a core (inner shell) electron. For each and every element, there will be a characteristic binding energy associated with each core atomic orbital i.e. each element will give rise to a characteristic set of peaks in the photoelectron spectrum at kinetic energies determined by the photon energy and the respective binding energies.

The presence of peaks at particular energies therefore indicates the presence of a specific element in the sample under study - furthermore, the intensity of the peaks is related to the concentration of the element within the sampled region. Thus, the technique is capable of yielding a quantitative analysis. The most commonly employed x-ray sources are those giving rise to:

- Mg K_α radiation: $h\nu$ = 1253.6 eV
- Al K_α radiation: $h\nu$= 1486.6 eV

The emitted photoelectrons will therefore have kinetic energies in the range of ca. 0 - 1250 eV or 0 - 1480 eV. Since such electrons have very short inelastic mean free paths in solids, the technique is necessarily surface sensitive. For an electron emitted towards the surface, there would be less chance of inelastic scattering before it escaped from the solid. XPS is not completely surface specific though, in that whilst most of the signal comes from within a few atomic layers of the surface, a small part of the signal comes from much deeper into the solid.

In this study, the chemical state of tungsten, oxygen and additives has been analysed by XPS. The spectra were obtained on a Physical electronics 5500 spectrometer, using monochromatic Al K α radiation (1486.6 eV). All spectra were taken at room temperature and tungsten oxide samples were mounted to be in adequate electric contact with the holder. Measurement conditions and parameters were verified to get the right carbon peak position (C 1s = 248.8 eV), assuming an error lower than 0.2 eV**.** Spectra were fitted with Gaussian-Lorentzian (80-20% respectively) peaks, considering a Shirley baseline. More references about XPS can be found in [12,13].

2.2.4 Diffuse reflectance infrared Fourier transformed spectroscopy

Diffuse Reflectance spectroscopy (DRS) is a spectroscopic technique based on the refection of light in the ultraviolet (UV), visible (VIS) and near-infrared (NIR) region by a powdered sample. In this study we have limited to DRIFT spectroscopy (Diffuse Reflectance Infrared Fourier Transformed).

In a DRS spectrum the ratio of the light scattered from an infinitely thick layer and the scattered light from an ideal non-absorbing reference sample is measured as a function of the wavelength. The illumination of powdered samples by incident radiation leads to diffuse illumination of the samples. The incident light is partially absorbed, partially scattered. The scattered radiation, emanating from the sample is collected in an integration sphere and detected.

One of the main advantages of this technique is that it can be operated under controlled conditions of temperature and ambience gases. Fig. 2a shows a typical diffuse reflection attachment for in situ measurements. Its construction with two ellipsoidal mirrors provides that mainly the diffuse component of the reflected light is captured [8]. In conjunction with this attachment, a stainless steel reaction chamber (Fig. 2b) can be used with quartz

windows and with gas ports for evacuating the chamber and/or for introducing gas. The chamber can be used under static or dynamic conditions.

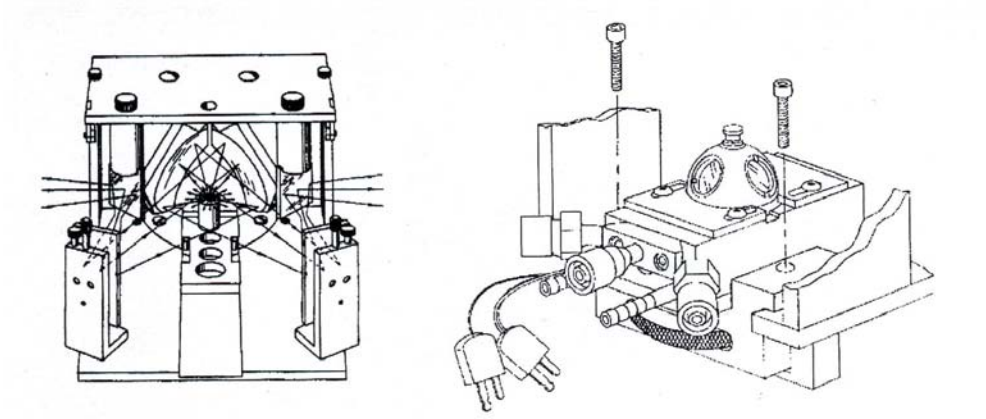

Fig 2: *In-situ DRS cell: (left) diffuse reflection attachment and (right) stainless steel reaction chamber (After [14]).*

In practice, diffuse reflection spectra are complex and are strongly dependent upon the conditions under which they are obtained. These spectra can exhibit both absorbance and reflectance features due to contributions from transmission, internal and specular reflectance components as well as scattering phenomena in the collected radiation. Diffuse reflectance spectra are further complicated by sample preparation, particle size, sample concentration and optical geometry effects, to name a few. Finally, it is common to take as a reference the spectrum of a mirror and reference sample spectra to this one.

In this study, DRIFTS has been applied to study the superficial vibrations of WO_3, specially the terminal W=O bonding, hydroxyl groups and the vibrations of adsorbed ammonia on WO_3-based powders. The spectra were obtained using a Nicolet 510P infrared spectrometer, with KBr optics and a DTGS detector. A controlled environment reflectance cell (Spectra-Tech 0030-101), equipped with ZnSe windows, was coupled to the spectrometer. More information about the principles of this technique and applications can be found in [14].

2.2.5 Raman spectroscopy

The scattering mechanisms between an incident radiation and a certain substance can be classified on the basis of the difference between the energies of the incident and scattered

photons. Briefly, if the energy of the incident photon is equal to that of the scattered one, the process is called Rayleigh scattering. If the energy of the incident photon is different to that of the scattered one, the process is called Raman scattering.

In crystalline solids, the Raman effect deals with phonons. A phonon is Raman-active only if the first derivative of the polarizability with respect the vibrational normal co-ordinate has a non-zero value, and this in turns depends by the crystal symmetry. A phonon can be either IR or Raman active only in crystals without centre of inversion. For every crystal symmetry class, is possible to calculate which phonons are Raman active, and in which measurement geometry, i.e. for which direction of polarisation of the incident and scattered light, relative to the crystallographic axis, also using the Raman tensors tabulated in many texts. Performing measurements in controlled polarisation configurations is possible to obtain information about the symmetry of the crystalline lattice. The Raman signal is very weak: only 1 photon in 10^7gives rise to the Raman effect. The Raman spectra are usually plotted in intensity vs. the difference in wave number between the incident beam and the scattered light, and so peaks are in correspondence to the phonon frequency. In nanocrystalline materials, Raman features are broadened and shifted by the phonon confinement. By using an adequate model, is possible to estimate the size of the nanocrystals. From the band-shifts and the presence of "forbidden" peaks, using the Raman spectroscopy is also possible to obtain information on the disorder and the strains present in the crystalline lattice.

In this investigation, information on the structural properties of WO_3, and of additives in some cases, have been obtained by Raman spectroscopy. Raman scattering measurements were obtained in backscattering geometry with a Jobin-Yvon T64000 spectrometer coupled to an Olympus metallographic microscope. Excitation was provided by an argon-ion laser operating at a wavelength of 457.5 nm with a low incident power to avoid thermal effects. Raman shifts were corrected by using silicon reference spectra after each measurement. General references about Raman spectroscopy can be found in [15,16].

2.2.6 Electron paramagnetic resonance

Electron Paramagnetic Resonance (EPR), often called Electron Spin Resonance (ESR), is a branch of spectroscopy in which electromagnetic radiation (usually of microwave frequency) is absorbed by molecules, ions, or atoms possessing electrons with unpaired spins, i.e. electronic spin $S > 0$, which is a common feature of transition metals. This

technique can provide information about the geometry of the EPR active species as well as information about its electronic structure.

The sample material is immersed in a strong static magnetic field and exposed to an orthogonal low- amplitude high-frequency field. EPR usually requires microwave-frequency radiation (GHz). The energy is absorbed by the sample when the frequency of the radiation is appropriate to the energy difference between two states of the electrons in the sample, but only if the transition satisfies the appropriate selection rules. This is its main limitation, but sometimes its great advantage.

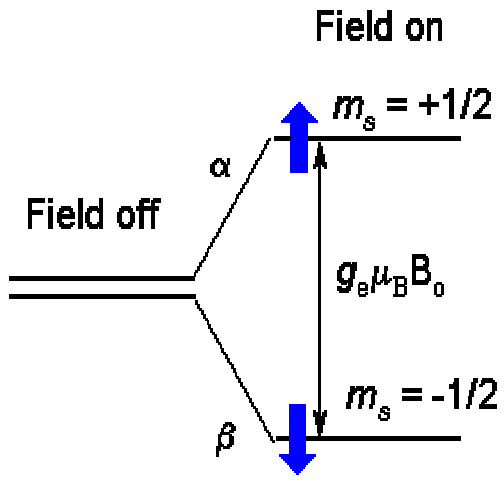

Fig. 3: Different projections of the spin lead to different energies in the presence of a magnetic field (Zeeman effect) [17]

Fundamental Principles

In EPR, because of the interaction of the unpaired electron spin moment (given by two projections, $m_s = \pm 1/2$, for a free electron) with the magnetic field, the so-called Zeeman effect, different projections of the spin gain different energies, as shown on Fig. 3:

$$E_{m_s} = g_m \mu_B B_0 m_s \qquad (1)$$

Here B_o is the field strength of the external magnetic field. The SI unit for the magnetic field is tesla, T, but, historically in EPR, gauss (1G = 0.0001 T) is still used. Other terms in Eq (1): m_s - is a spin projection on the field ($m_s = \pm 1/2$ for a free electron), μ_B is the Bohr magneton:

$$\mu_B = \left| eh / 4\pi m_e \right| = 9.2740 \times 10^{-24} J/T \qquad (2)$$

with e and m_e being electron charge and mass, respectively, and h-Planck's constant. Parameter g for free electron, g_e, has the value close to two: (g_e =2.0023193). If the electron has nonzero orbital angular moment, L, the g-value (sometimes called factor Landé) becomes:

$$g = 1 + \frac{S(S+1) - L(L+1) + J(J+1)}{2J(J+1)} \quad (3)$$

The overall magnetic momentum, μ_{eff}, can be expressed via overall angular momentum, *J*, and the g-value:

$$\mu_{eff} = g\mu_B\left[J(J+1)\right]^{1/2} \quad (4)$$

For most of organic radicals and radical ions, unpaired electrons have *L* close to zero and the total electron angular momentum quantum number *J* is pretty much the spin quantum number, *S*. As result, their g-values are close to 2. Situation becomes much more complicated with transition metals. Not only they have large *L*'s and *S*'s, but these values depend on the surrounding electric fields of ligands, making everything messier but also more interesting. If *L* = 0 then J = S, and Eq. (1) will define the energies of all the possible projection of m_s from -*S* to *S* - 1, *S* (2*S* + 1 of such).

If the molecule contains nuclei with magnetic moments, such as protons, their interaction with external field and the electronic magnetic moment will change stationary energies of Eq.(1). The nuclear angular momentum quantum number *I* determines the nuclear magnetic moment the same way as for the electron:

$$\mu = g_N\mu_N\left[I(I+1)\right]^{1/2} \quad (5)$$

with μ_N now being the nuclear Bohr magneton:

$$\mu_N = \left|eh/4\pi m_p\right| = 5.051\times10^{-27}\,J/T \quad (6)$$

much smaller value because of the ~2000 times more heavier proton m_p. The nuclear *g* factor, g_N, is obtained from a knowledge of the structure of the nucleus. Interaction with external field splits the nuclear sublevels due to Zeeman interaction the same way as for electron spin:

$$E_{m_I} = g_N\mu_N B_0 m_I \quad (7)$$

where m_I is one of the 2*I* + 1 projections of the nuclear spin. Electron-nuclear interaction will depend on the projections of both, electron and nuclear spins:

$$E_{electron-nuclear} = Am_I m_S \quad (8)$$

where coefficient A, a so-called hyperfine coupling constant/interaction (hfi), depends not only on the g-values for the electron and the nucleus but also on the distance between them and their orientation with respect to the external field (dipole-dipole interaction). In solutions, the anisotropic part of this interaction averages out because of the fast molecular rotation. The remaining isotropic part is given by the Fermi contact interaction in the form:

$$A = (8\pi/3) g_N \mu_N g_e \mu_B \rho(0) \quad (9)$$

where $\rho(0) = |\psi(0)|^2$ is the unpaired electron density at the nucleus. For pure 1s electron on hydrogen atom, A equals h x 1420 MHz. As a matter of convenience, hyperfine constants are usually given in Gauss, $a = A/g_e\mu_B$. For example, hydrogen it corresponds to a = 508 G. Summing up all energies, we arrive at modified Eq. (1)

$$E = g_e m_B m_S \left(B_0 + \sum a_i m_{Ii}\right) - g_N \mu_N B_0 m_I \quad (10)$$

Experimental

A typical spectrometer consists of an electromagnet with power supplies to generate and modulate a uniform magnetic field of several thousand Gauss, as well as the components that generate and detect microwave power. A static magnetic field is provided by an electromagnet with a current- regulated power supply. A homogeneous field is required for best results. A Hall probe, driven from a stable constant-current power system, with a digital multimeter (DMM) reading the Hall voltage, is used to measure the value of the magnetic field between the poles of the magnet.

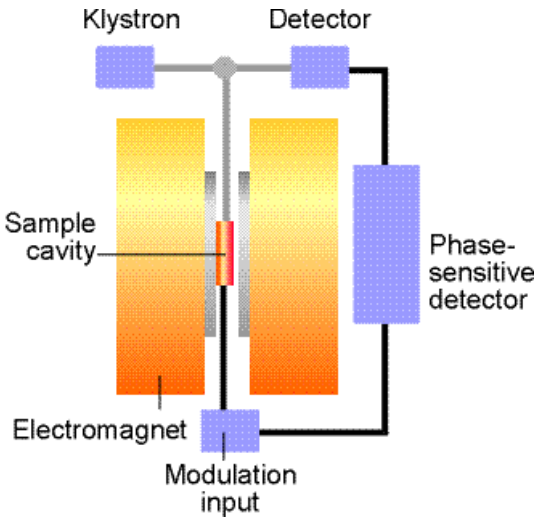

Fig. 4: *Schematic diagram of a typical EPR apparatus (After [17])*

The microwave system consists of a microwave power supply that uses a

clystron (Fig. 3). The output of the microwave power (mw) supply is connected via rectangular wave-guide and through a circulator to a high-Q resonant cavity. The samples to be investigated are mounted in the middle of the cavity, where magnetic component of the microwave power has a maximum. A microwave diode, which detects the mw resides inside the same box as the power supply. The higher the quality of the resonant cavity, the greater the microwave field can be obtained on the sample.

There are varieties of schemes for detecting resonant EPR transitions. Historically, most popular became a detection of absorption of the microwave power. To minimise the noise from the mw diode in steady state measurements, a magnetic field modulation scheme with phase sensitive detection is usually employed. As a result, the detected signal appears as a first derivative (Fig. 4).

The time the unpaired electron stays in the higher energy state before relaxing back to the lower energy state is called the lifetime. The lifetime is inversely proportional to the line width of the EPR resonance due to the uncertainty principle. The longer the lifetime the narrower the resonance. Lifetimes for EPR vary between 10^{-4} and 10^{-8} seconds. Since lifetimes increase as the temperature of the system is lowered, it is common to cool EPR samples to liquid nitrogen (77K) or liquid helium temperatures (4K) in order to observe an EPR signal.

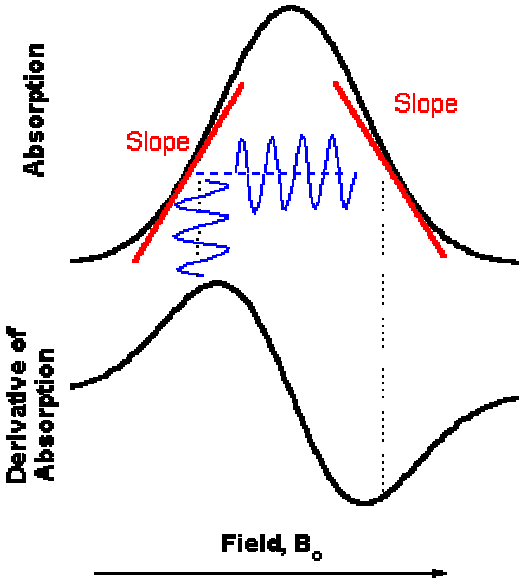

Fig. 5: Absorption and derivative of the absorption (detected signal) in a typical EPR measurement [17]

Applications

Whereas EPR is not a common characterisation technique in the field of gas sensors based on metal oxides, it has been widely used in the field of heterogeneous catalysis for more than 30 years. However, it is well known that these two fields are closely related, so most of the following applications could be also useful in the case of gas sensors based on metal oxides:

- Detection of adsorbed paramagnetic species
- Paramagnetic species introduced in the material in order to "probe" the material via EPR parameter response (racers)
- Surface properties giving rise to paramagnetic species
- Bulk properties as evidenced by ionisation of bulk atomic arrangements using uv light from a mercury lamp or γ rays from a ^{60}Co source
- Transition metal ions within or at the surface of a material

In this study, chemical state of the additives has been analysed by EPR. The X band CW-EPR spectra were recorded at 123K on a Bruker EMX spectrometer, using 5 mW microwave power and 5G-modulation amplitude. The temperature control in the range 300-4 K was achieved through an Oxford cryostat for X band spectrometer. Thermal treatments of the dried gel samples were performed at 673 K and 973 K, under dry flowing air, in a quartz apparatus suitable for both gas-flow and EPR measurements, so as to avoid contact with uncontrolled atmosphere. The g values were measured by standardisation with diphenylpicrylhydrazyl (DPPH). References about EPR characterisation of transition metal chemistry and materials for catalysis can be found in [18-20].

2.2.7 Temperature programmed desorption

Temperature programmed desorption (TPD) or thermal desorption spectroscopy (TDS), as it is also called, is particularly useful in surface science, where one studies the desorption of gases from single crystals and polycrystalline foils into vacuum.

First of all, some concepts and vocabulary concerning this technique should be clarified. When a gas or vapour is brought into contact with a solid, the solid takes up part of it. The molecules that disappear from the gas either enter the inside of the solid, or remain on the outside attached to the surface. The former phenomenon is termed *absorption* (or dissolution) and the latter *adsorption*. When the phenomena occur simultaneously, the process is termed *sorption*. The solid that takes up the gas is called the *adsorbent*, and the gas or vapour taken up on the surface is called the *adsorbate*.

Molecules and atoms can attach themselves onto surfaces in two ways. In *physisorption* (physical adsorption), there is a weak van der Waals attraction of the adsorbate to the surface. The attraction to the surface is weak but long ranged and the energy released upon

accommodation to the surface is of the same order of magnitude as an enthalpy of condensation (on the order of 20 kJ/mol). During the process of physisorption, the chemical identity of the adsorbate remains intact, i.e. no breakage of the covalent structure of the adsorbate takes place.

In *chemisorption* (chemical adsorption), the adsorbate sticks to the solid by the formation of a chemical bond with the surface. This interaction is much stronger than physisorption, and, in general, chemisorption has more stringent requirements for the compatibility of adsorbate and surface site than physisorption. The chemisorption may be stronger than the bonds internal to the free adsorbate, which can result in the dissociation of the adsorbate upon adsorption (dissociative adsorption). In some cases, dissociative adsorption can be greater than zero, which means endothermic chemisorption, although uncommon, is possible.

The basic experiment has two main parts:

- Adsorption of one or more molecular species onto the sample surface at a certain temperature
- Heating of the sample in a controlled manner (preferably so as to give a linear temperature ramp) whilst monitoring the evolution of species from the surface back into the gas phase with a gas chromatograph and a mass spectrometer (GC-MS).

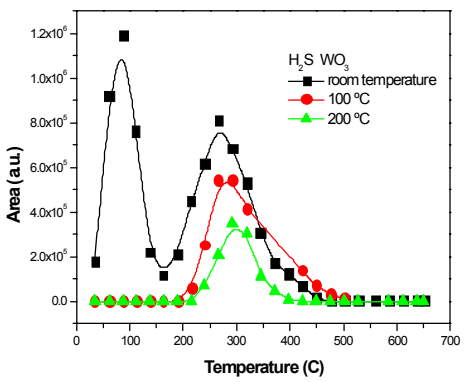

Fig. 6: TPD of H_2S, preadsorbed at different temperatures, from WO_3 nanocrystalline powder

The data obtained from such an experiment consists of the intensity variation of each recorded mass fragment as a function of time (temperature). It must be pointed out that if adsorbate molecules do react on the surface of the sample, reactions products may also be detected.

Fig. 6 shows data from a typical TPD experiment (H_2S on nanocrystalline WO_3). The following points are worth noting:

- The area under a peak is proportional to the amount originally adsorbed, i.e. proportional to the surface coverage.
- The kinetics of desorption (obtained from the peak profile and the coverage dependence of the desorption characteristics) give information on the state of aggregation of the adsorbed species
- The position of the peak (the peak temperature) is related to the enthalpy of adsorption, i.e. to the strength of binding to the surface. The higher the temperature is, the stronger the binding is.

The complete desorption analysis can be very complicated, so many authors rely on simplified methods to obtain certain parameters such as the activation energy of desorption. These methods make use of easily accessible spectra features (temperature of the peak maximum, half width at half maximum of the peak). The most popular is the Readhead method [21]:

$$E_{des} = RT_{max}\left[\ln\left(\frac{\nu T_{max}}{\beta}\right) - 3.46\right] \qquad (11)$$

where

E_{des} is the activation energy of desorption

R is the gas constant

T_{max} is the peak maximum temperature

ν is the preexponencial factor

β is the heating rate, dT/dt

This expression is approximately correct for first-order desorption and for values of ν/β between 10^8 and 10^{13} K^{-1}. The critical point is that one value for ν must be chosen, the general choice being 10^{13} s^{-1}

Another popular method has been developed by Chan, Aris and Weinberg [22]. Their expressions for first order desorption are:

$$E_{des} = RT_{max}\left[-1 + \sqrt{1 + 5.832\left(\frac{T_{max}}{W}\right)^2}\right] \qquad (12)$$

$$\nu = \frac{E_{des}\beta}{RT_{max}^{2}} e^{E_{des}/RT_{max}} \qquad (13)$$

in which *W* is the peak width at half maximum intensity.

In this study, the desorption of ammonia and hydrogen sulphide from pure and catalysed WO_3 have been analysed by TPD. WO_3-based powder was pressed into discs and then crushed into granules (40-60 mesh). These granules (3 g) were introduced in a glass reactor connected to a flow apparatus. Before NH_3 or H_2S adsorption, granules were pre-treated in synthetic air (50 ml/min) at 650ºC for 1 hour. Afterwards, temperature was decreased to the adsorption temperature (room temperature, 100ºC and 200ºC). At this temperature, a flow of NH3 or H2S balanced with air (100 ml/min) passed through the reactor for 3 hours. Then the flow was changed to He (10 ml/min) and the granules were quenched to room temperature. Finally, temperature was increased from room temperature to 650ºC at a rate of 5ºC/min in the same He stream. The desorbed species were analysed by a gas chromatography-mass spectrometer (GC-MS, Shimadzu, QP-5000) with a Pora PLOT Q column (Chrompack) during TPD runs. Further readings can be found elsewhere [14].

2.3 Gas sensors

2.3.1 Fabrication of the sensors

Thick-film gas sensors were obtained by screen-printing of a paste based on the obtained powder over alumina substrates.

After annealing the WO_3-based powder, a paste was obtaining by mixing the powder with an appropriate amount of an organic vehicle until a homogeneous paste is observed. This paste is placed over the screen of the printing machine.

Planar alumina substrates were used as sensor substrates. These substrates had previously printed electrodes and heater, both of platinum. Electrodes were interdigitated, with a width of 0.3mm and a distance of 0.2mm. The paste was printed by using a semi-automatic printing machine.

After the printing, sensors were left at room temperature for a couple of hours so as to settle down the paste. They were then heated at 100ºC for a day to dry the paste. Before any test, sensors were heated for a day at 350ºC inside the test chamber under a flow of 200 ml/min of synthetic air.

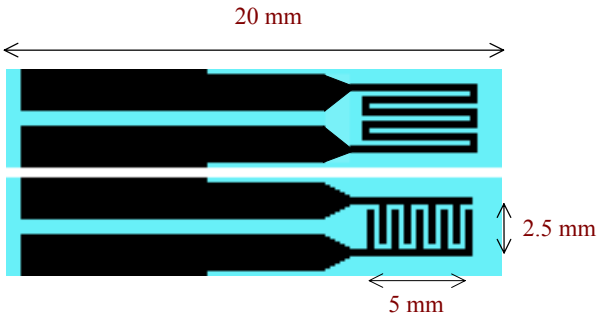

Fig.7: *Schematic layout of the alumina substrates. (top) Back side of the substrate, with the platinum heater. (bottom) Front side of the substrate, with the interdigitated electrodes.*

2.3.2 Test system

Sensors were placed in a stainless steel test chamber (200 ml). A continuous flow of gas (200 ml/min) passes through the chamber, which makes the pressure in the test chamber to be nearly atmospheric. The desired gas concentration is obtained by mixing the appropriate

flows of gases by means of mass flow controllers (Bronkhorst F201C). Humidity was controlled by mixing the appropriate quantities of dry air with water-bubbling air, monitoring the relative humidity with a commercial capacitive humidity sensor. The same computer using acquisition boards (Computerboards CIO-DAC08/16 and CIO-DAS1602/16) performed the acquisition. More details about the test system can be found in [23].

2.4 References

[1] J. H. Kim and K. L. Kim, *A study of preparation of tungsten nitride catalysts with high surface area*, Appl. Catal. A 181 (1999) 103-111.

[2] C. Balázsi, M. Farkas-Jahnke, I Kotsis, L. Petrás, J. Pfeifer, *The observation of cubic tungsten trioxide at high-temperature dehydration of tungstic acid hydrate*, Solid State Ionics 141-142 (2001) 411-416.

[3] M. Akiyama, J. Tamaki, N. Miura and N. Yamazoe, *Tungsten oxide-based semiconductor sensor highly sensitive to NO and NO_2*, Chem. Lett., (1991) 1611-1614.

[4] J. Tamaki, Z. Zhang, K. Fujimori, M. Akiyama, T. Harada, N. Miura and N. Yamazoe, *Grain-size effects in tungsten oxide-based sensor for nitrogen oxides*, J. Electrochem. Soc., 141 (1994) 2207-2210.

[5] H.P. Klug, L.E. Alexander, *X-ray diffraction procedures*, John Wiley and Sons Inc., New York, 1954.

[6] R. Jenkins, Instrumentation, in Reviews in Mineralogy vol. 20: *Modern Powder Diffraction*, ed. DL. Bish and J.E. Post, The Mineralogical Society of America, Washington, D.C., pp 19-43 (1989).

[7] B.E. Warren, *X-ray Diffraction*, Dover publications, Inc., New York (1990).

[8] D.B. Williams and C.B. Carter (ed.), *Transmission electron microscopy: a textbook for materials science*, Plenum Press, New York (1999).

[9] A. Diéguez, *Structural analysis for the improvement of SnO_2-based gas sensors*, Ph.D. Thesis, Universitat de Barcelona (1999).

[10] M. José-Yacamán, G. Díaz, A. Gómez, *Electron microscopy of the catalysts: the present, the future and the hopes*, Catalysis Today 23 (1995) 161-199.

[11] J. Arbiol*, Metal Additive Distribution in TiO_2 and SnO_2 Semiconductor Gas Sensor Nanostructured Materials*, Ph.D. Thesis, Universitat de Barcelona (2001).

[12] J.F. Moulder, W.F. Stickle, P.E. Sobol, K.D. Bomben, *Handbook of X-ray Photoelectron Spectroscopy*, ed. J. Chastain, Perkin-Elemer Corp., Minnesota (1979).

[13] D. Briggs, M.P. Seah, *Practical Surface Analysis vol 1: Auger and X-ray Photoelectron Spectroscopy*, John Wiley and Sons, Chichester (1990).

[14] Bert M. Weckhuysen, Robert A. Schoonheydt, *Recent progress in diffuse reflectance spectroscopy of supported metal oxide catalysts*, Catalysis Today 49 (1999) 441-451

[15] N.B. Colthup, L.H. Daly, S.E. Wiberly, *Introduction to infrared and Raman spectroscopy*, Academic Press Inc., New York and London, 1st ed. 1964 and 3rd ed. 1990.

[16] J.G. Grasselli. B.J. Bulkin, *Analytical Raman Spectroscopy*, John Wiley and Sons Inc., New York (1991).

[17] New Mexico State University, Department of Chemistry and Biochemistry, http://www.chemistry.nmsu.edu/studntres/chem435/Lab7/intro.html

[18] J.C. Vedrine, in : F. Delannay (Ed.), *Characterization of heterogeneous catalysts*, Dekker, New York (1984) p.161.

[19] K. Dyrek, M. Che, *EPR as a tool to investigate the transition metal chemistry on oxide surfaces*, Chem Rev. 97 (1997) 305-331.

[20] Z. Sojka, M. Che, Catalytic chemistry of transition metal ions on oxide surfaces. A molecular approach using EPR techniques, C.R. Acad. Sci. Paris, Série IIc, Chimie/Chemistry 3 (2000) 163-174.

[21] P.A. Redhead, Vacuum 12 (1962) 203.

[22] C.M. Chan, R. Aris, W.H. Weinberg, Appl. Surface Sci. 1 (1978) 360.

[23] A. Cirera, *New technologies and their characterisation for nanostructured SnO_2 gas sensor devices*, Ph.D. Thesis, Universitat de Barcelona (2000).